Evaluating Different Methods for the Estimation of Bare Soil Surface Reflectance Using Multispectral Satellite Image Time Series

Eleni Sofikiti [1], Vasileios Tsironis [1], Konstantinos Karantzalos [1]

[1]Remote Sensing Laboratory, National Technical University of Athens, 15780 Zographos, Greece - elsofikiti@mail.ntua.gr, {tsironisbi, karank}@central.ntua.gr

Keywords: Bare soil composite, Spectral reflectance, Soil, Landsat 8.

Abstract

Soil degradation poses a significant threat to both food security and climate change. Remote Sensing offers valuable insights for soil monitoring, enabling cost-effective observation across extensive regions and extended periods of time. This study evaluates bare soil reflectance mapping at medium spatial resolution by benchmarking the performance of various compositing approaches, providing an assessment of the contribution of different techniques i.e., simultaneous use of multiple spectral indices, different compositing, masking or thresholding techniques and other parameters of the time series i.e. cloud cover and time range. Focusing on Greece, a Mediterranean country with diverse microclimates and soil types, the study leverages Landsat 8 images spanning from 2015 to 2020 and the LUCAS 2015 database to evaluate the results. A wide range of experiments were conducted to determine the best approach for creating a bare soil reflectance composite (BSC), evaluated based on a) its correlation per spectral band with the spectral reference data and b) its performance in soil organic carbon prediction, serving as an indicator of the BSC's quality. The study demonstrated that estimating bare soil reflectance from multispectral satellite image time series can be significantly improved through careful selection and optimization of a range of parameters especially over a large and heterogeneous study area. The results offer a strong basis for refining methodologies in bare soil reflectance estimation and provide insightful information for future monitoring efforts.

1. Introduction

Soil, as a natural resource, is essential for food production and plays a crucial role in achieving climate neutrality. Soil degradation is a growing problem that necessitates action, prompting the European Union (EU) and United Nations (UN) to implement policies for its continuous monitoring (Panos Panagos, 2024). In this context, there is a rising demand for current and comprehensive soil information to support climate change monitoring, policy-making decisions and the adoption of agricultural practices aligned with these policies.

In the context of soil monitoring, Remote Sensing can provide valuable insights by enabling cost-effective monitoring of crops and soil across large areas and over long periods of time (Beth Delaney, 2025). Medium spatial resolution satellite data have been employed to produce bare soil surface reflectance maps used to predict valuable soil properties such as soil Organic Carbon (OC) content (Simone Zepp, 2023) (Tom Broeg, 2024) (Fabio Castaldi, 2023). Key challenges in this method include distinguishing soil from vegetation, especially crop residue, while minimizing the influence of soil moisture (Klara Dvorakova P. S., 2020) and surface roughness on the reflectance of bare soil (Diego Urbina-Salazar, 2023). Additionally, our study encompasses a large geographical extent, spanning the national level, which is characterized by highly heterogeneous landscapes, significant land cover diversity as well as different climate zones (Karakizi, 2018). In this case the methodology used needs to account for the challenges that come with large soil type and crop managemend technics variability (Tom Broeg, 2024), (Jie Xue, 2024), (KARAKIZI, 2024).

Generally, most works rely on several satellite spectral indices to distinguish bare soil (Beth Delaney, 2025) but few studies are dedicated to evaluating and comparing all the different approaches for the adequate estimation of bare soil reflectance from satellite imagery. The goal of this work is to thoroughly evaluate the accurate bare soil reflectance mapping in Greece at medium spatial resolution, by investigating the effectiveness of different compositing approaches. A comprehensive evaluation of the contribution of simultaneous use of multiple spectral indices, different compositing, masking or thresholding techniques and other time series parameters tuning, such as cloud cover and time range, is performed.

This study contributes to the field of bare soil mapping by systematically evaluating the effectiveness of bare soil reflectance composites (BSCs) generated using various spectral indices, parameters and thresholding techniques applied to Landsat 8 (L8) time series. By incorporating dynamic thresholding with multiple spectral indices this study investigates the potential for enhancing the quality of BSCs while maintaining high spatial coverage, which is crucial given the large extent and high heterogeneity of the study area. Furthermore, this study emphasizes the sensitivity of the resulting BSCs when different methods are used and investigates the critical role of index selection in optimizing bare soil detection.

2. Source materials & Compositing methodology

2.1 Study Area

This study focuses on Greece at the national scale. The climate in Greece is Mediterranean, characterized by mild, wet winters and relatively warm summers. However, due to the country's unique geography, Greece exhibits a remarkable range of microclimates and local variations (Karakizi C. K., 2021). The climate is divided into two main periods: the cold, wet winter period from mid-October to late March, and the dry period from April to October. Temperatures in the mainland range from -5 to +5°C during the coldest month, January, and up to 8°C in the islands. During the warmest part of the year, from late July to

This contribution has been peer-reviewed.
https://doi.org/10.5194/isprs-archives-XLVIII-M-7-2025-207-2025 |

mid-August, temperatures average between 29 and 35°C. Spring is brief with low temperatures, while autumn is characterized as long and cool. The country receives from 350 to 1200 mm of rain per year depending on the area (Hellenic National Meteorological Service, 2025). The main reference soil groups in Greece are Fluvisols, Cambisols, Gleysols, Luvisols, Calcisols, Regosols, Vertisols, Leptosols, and Histosols (OPEKEPE, 2015)

2.2 Validation Data

To evaluate the results LUCAS 2015 database (Gergely Tóth, 2013), created by the European Soil Observatory, was utilized. This database includes data on soil properties such as clay, silt, and sand content, organic carbon (OC), calcium carbonate ($CaCO_3$), and other attributes, along with reflectance data and auxiliary information for each sample, such as land use and reference soil group. Specifically for Greece, the database includes 641 samples. For the purposes of this study, the soil reflectance data and OC content [g Kg-1] of each sample were utilized. The spectral reflectance of the samples includes measurements across the visible, infrared, and shortwave infrared parts of the spectrum (400–2500 nm) with a spectral resolution of 0.5 nm. To compare the spectral reflectance reference data from LUCAS 2015 database with the spectral reflectance from L8, resampling of reflectance to match the spectral specification of L8 bands was performed (Uta Heiden, 2022).

2.3 Landsat 8 and Auxiliary Data

Our workflow was based on L8 time series and auxiliary datasets that were accessed, processed and exported via Google Earth Engine (GEE) (Gorelick, 2017). We utilized all available L8 Level 2, Collection 2, Tier 1 Surface Reflectance images over the study area spanning from 2015 to 2020 with cloud cover less than a set threshold (typically set to 30%). Each image was masked with the quality band of L8. Using ESA World Cover 10m v100 2020 and Copernicus CORINE Land Cover 2018 datasets available on GEE only areas characterized as Grassland, Cropland and Bare / Sparse Vegetation were included for further analysis.

2.4 Methodology

A wide range of experiments were conducted to determine the best approach to create a BSC that a) shows the highest correlation per spectral band with the spectral reference data of LUCAS 2015 and b) achieves improved performance in regards of soil OC prediction using the LUCAS 2015 dataset. This study evaluates the use of Normalized Difference Vegetation Index (NDVI), Normalized Burn Ratio 2 (NBR2) (José Alexandre Melo Demattê, 2018), Bare Soil index (BSI) (Sanne Diek, 2017), Soil Surface Moisture Index (S2WI) (Emmanuelle Vaudour C. G., 2019) spectral indices, used both individually and in various combinations, in order to test their ability to distinguish bare soil (BS) pixels from vegetation and crop residue while minimizing the influence of soil moisture.

Additionally simple thresholding, i.e. setting a single threshold value for the entire area of interest, and dynamic thresholding (Tom Broeg, 2024), i.e. different threshold for each pixel, were tested. Different thresholds for the indices were tested and different compositing methods i.e., mean (Anis Gasmi, 2021), median (José Alexandre Melo Demattê, 2018), min NDVI, min NBR2, min S2WI or max BSI (Emmanuelle Vaudour C. G.-S., 2021), (Sanne Diek, 2017), (Fabio Castaldi, 2023). Additionally, we investigated the optimal maximum cloud cover threshold for filtering the image time series and whether setting a minimum number of BS instances (Tom Broeg, 2024) for the pixels included in the BSC improves the results. Finally, all approaches were tested for a 1-year (Castaldi, 2021) or a 6-year (Diego Urbina-Salazar, 2023) long time series.

2.4.1 Experimental setup

After the creation of L8 time series over the study area, for each cloud-free, quality and land cover masked L8 image the four spectral indices were computed and added to the collection. Then the L8 time series was masked to identify BS. To this end, two different thresholding methodologies were tested; first the fixed thresholding method was tested where one threshold is applied to the entire time series. Fixed thresholding was tested with different combinations of the four spectral indices. Three commonly used thresholds were examined for the NDVI and NBR2 spectral indices, respectively (Nélida Elizabet Quiñonez Silvero, 2021), (José Lucas Safanelli, 2020), (José Alexandre Melo Demattê, 2018), (Castaldi, 2021), (Cécile Gomez, 2022). For BSI and S2WI there are not widely used thresholds in the literature, instead they are often used in a maximum BSI or minimum S2WI set up (Fabio Castaldi, 2023), (Emmanuelle Vaudour, 2021), (Sanne Diek, 2017) and (Emmanuelle Vaudour C. G., 2019). The maximum BSI and minimum S2WI values across the entire study area exhibited substantial variability upon visual inspection. Therefore, to prevent the unintentional exclusion of specific soil types, the absolute threshold values were deliberately set to be lenient.

Second, dynamic thresholding was tested with different combinations of the four spectral indices to evaluate its ability to detect BS pixels without significant reduction of the BSC's coverage or exclusion of specific soil types and conditions. First, the fixed thresholding was applied, and then the 40^{th} and 60^{th} percentiles of each pixel's band values were computed. For NBR2 and S2WI, pixels in the time series with values below the 40^{th} percentile were kept and for BSI, pixels with values over the 60^{th} percentile were kept. Pixels that passed both fixed and dynamic thresholding constitute the BS instances time series.

Regarding BS compositing, minimum BS instance thresholding was tested, wherein pixels with only a single BS observation were excluded from the final BSC. Then the different compositing methodologies were tested. From each BS instances time series, different BSCs were created computing the mean or median of all BS instances for each pixel. Also, only for the BS instances time series that were created with fixed thresholding the min NDVI, min NBR2, min S2WI, max BSI pixels were selected to create the final BSC.

The BS time series and BSCs created for the experiments were sampled with the LUCAS 2015 sampling points in GEE. The evaluation of the BSCs and the soil OC prediction models were developed locally in a python environment.

2.4.2 Evaluation

To evaluate the resulting BSCs two approaches were used; first the spectral reflectance of the BSC for each L8 band was compared to the spectral reflectance of the LUCAS 2015 spectral reference data in terms of Pearson's correlation coefficient, Root Mean Square Error (RMSE) and unbiased Root Mean Square Error (ubRMSE). Second, the BSCs were tested in their ability to predict soil OC content by employing four Machine Learning (ML) algorithms (Linear Regressor (LR), Kernel Ridge Regressor (KR), Random Forest Regressor (RF) and Support Vector Regressor (SVR)) using the BSC's L8 bands and 6

https://doi.org/10.5194/isprs-archives-XLVIII-M-7-2025-207-2025

spectral indices as training features and the LUCAS 2015 soil OC content as reference training and validation data.

NDVI, NBR2, BSI and S2WI were calculated from the BSC's reflectance and were used as predictors for the soil OC regression models. Plus, PVBlue and PVIR2 spectral indices (Simone Zepp, 2023) were calculated from the BSC reflectance and were also used as predictors. The best hyper parameters for the ML models were identified using grid search. The validation was performed assuming a 0.8-0.2 train-test split.

3. Results

First, the evaluation of different parameters for the BSC creation is performed by comparing the resulting 1-year BSCs in terms of correlation with LUCAS 2015 spectral reflectance. Next, we evaluate dynamic thresholding performance for 1-year and 6-year BSCs in terms of correlation with LUCAS 2015 spectral reflectance. Lastly, we evaluate the 6-year BSCs' ability to predict soil OC employing four ML models.

3.1 BSC spectral reflectance

First the use of different fixed threshold values for the indices NDVI and NBR2 to identify BS pixels is evaluated along with the use of minimum number of BS instances to include a pixel in the final BSC (i.e. BS frequency). Results indicated that by increasing BS frequency, through low-frequency pixel elimination, yielded substantially better correlation with the reference data. In Table 1, all BSCs with minimum frequency set to 2, for each pixel to be included in the BSC, systematically yield higher correlation with the reference reflectance data. In addition, in Table 1 it is shown that best results are achieved with NBR2 threshold value 0.10, compared to higher values (0.20 or 0.30) in accordance with (José Alexandre Melo Demattê, 2018), while setting the NDVI threshold value lower than 0.30, results to decreased BSC coverage with no substantial increase in the correlation values.

Minimum number of BS instances (frequency)														
	1							2						
NDVI	**0.30**													
NBR2	Blue	Green	Red	NIR	SWIR1	SWIR2	Support	Blue	Green	Red	NIR	SWIR1	SWIR2	Support
0.30	0.23	0.27	0.32	0.43	0.54	0.52	193	0.47	0.51	0.49	0.56	0.61	0.60	178
0.20	0.23	0.28	0.32	0.43	0.54	0.52	192	0.47	0.51	0.50	0.58	0.62	0.59	176
0.10	0.42	0.49	0.54	0.60	0.74	0.70	101	**0.71**	**0.72**	**0.71**	**0.73**	**0.82**	**0.79**	**80**
NDVI	**0.25**													
NBR2	Blue	Green	Red	NIR	SWIR1	SWIR2	Support	Blue	Green	Red	NIR	SWIR1	SWIR2	Support
0.30	0.24	0.30	0.35	0.47	0.58	0.56	158	0.42	0.50	0.50	0.60	0.65	0.62	131
0.20	0.25	0.30	0.35	0.47	0.58	0.56	157	0.43	0.50	0.50	0.60	0.65	0.62	129
0.10	0.42	0.48	0.53	0.61	0.74	0.72	95	**0.74**	**0.73**	**0.72**	**0.75**	**0.84**	**0.81**	**71**
NDVI	**0.20**													
NBR2	Blue	Green	Red	NIR	SWIR1	SWIR2	Support	Blue	Green	Red	NIR	SWIR1	SWIR2	Support
0.30	0.20	0.23	0.30	0.44	0.62	0.57	90	0.43	0.47	0.49	0.58	0.65	0.62	60
0.20	0.20	0.23	0.30	0.44	0.62	0.57	90	0.43	0.47	0.49	0.58	0.65	0.62	60
0.10	0.40	0.45	0.51	0.61	0.75	0.71	61	0.67	0.65	0.66	0.73	0.82	0.76	45

Table 1: Pearson's Correlation Coefficient between BSC and reference reflectance values and number of samples, for different NDVI and NBR2 fixed threshold values and different minimum number of BS instances. The BSCs resulted from 1-year long L8 time series (2015). Indices used for masking: NDVI+NBR2+BSI, where -1<BSI<1, maximum 30% cloud cover.

Next, setting the values 0.30 and 0.10 for the NDVI and NBR2 threshold values, accordingly, the different indices combination used for BS masking, maximum cloud coverage and compositing methods are evaluated. In Table 2, correlation between BSC reflectance and reference data reflectance using different combinations of indices to perform the BS pixels masking is presented. Although adding NBR2 thresholding, decreases the coverage (support: number of samples from LUCAS 2015 database that overlap with the resulting BSC), the quality of the BSC is drastically improved. The additional application of BSI thresholding marginally enhances the quality of the BSC, as reflected by slightly higher correlation values. The marginal improvement is likely due to the BSI threshold being very lenient. Adding S2WI to the thresholding process did not improve the corelation with the reference data but that is likely due to the S2WI threshold values being lenient.

Indices combination	Blue	Green	Red	NIR	SWIR1	SWIR2	Support
NDVI	0.44	0.49	0.48	0.56	0.61	0.59	178
NDVI+NBR2	0.67	0.69	0.69	0.71	0.81	0.79	80
NDVI+NBR2+BSI	0.71	0.72	0.71	0.73	0.82	0.79	80
NDVI+NBR2+BSI+S2WI	0.71	0.72	0.71	0.73	0.82	0.79	80

Table 2: Pearson's Correlation Coefficient between BSC and reference reflectance values and number of samples, for different indices combinations used for the thresholding. The BSCs resulted from 1-year long L8 time series (2015). Minimum number of BS instances was set to 2. Fixed threshold values: 0<NDVI< 0.30, 0<NBR2 < 0.1, -1 <BSI <1, -0.8<S2WI<0, maximum 30% cloud cover.

The use of different maximum cloud coverage values to filter the L8 images that are included in the time series is also evaluated. The increase of maximum image cloud coverage from 30% to 50%, to include more input images to the BSC, did not improve the BSC's coverage, and further increase to 70% reduced the quality of the BSC due to residual errors in cloud masking algorithms (Table 3).

	Maximum cloud coverage [%]	Blue	Green	Red	NIR	SWIR1	SWIR2	Support
NDVI+NBR2+BSI	**30**	0.71	0.72	0.71	0.73	0.82	0.79	80
	50	0.72	0.73	0.72	0.74	0.82	0.80	80
	70	0.67	0.69	0.69	0.71	0.81	0.78	82

Table 3: Pearson's Correlation Coefficient between BSC and reference reflectance values and number of samples, for different maximum cloud cover values. The BSCs resulted from 1-year long L8 time series (2015). Minimum number of BS instances was set to 2. Fixed threshold values: 0<NDVI< 0.30, 0<NBR2 < 0.1, -1 <BSI <1, -0.8<S2WI<0, maximum 30% cloud cover.

In Table 4 the use of different compositing methods is evaluated. The highest correlation between BSC and reference reflectance is achieved using BSCs based on the mean and median compositing methods of all BS appearances in the time series. Calculating the mean or median of all BS appearances reduces the influence of extreme values in surface reflectance over time, which are typically caused by factors such as soil moisture, surface roughness, and residual vegetation that were not fully removed through index thresholding (Castaldi, 2021).

Creating a BSC by choosing the reflectance of the date with the minimum value of the S2WI, yielded the lowest correlation with the reference data. These results may be due to the low sensitivity of S2WI with the change in soil moisture conditions in time and are in accordance with (Emmanuelle Vaudour, 2021). Although mean and median methods yielded similar results, we opted for the mean compositing method, as visual inspection revealed it produced smoother results with limited appearance of salt and pepper noise.

Compositing method	Blue	Green	Red	NIR	SWIR1	SWIR2
Mean	0.71	0.72	0.71	0.73	0.82	0.79
Median	0.72	0.73	0.71	0.71	0.81	0.78
Min BSI	0.63	0.64	0.65	0.62	0.73	0.70
Min NBR2	0.63	0.65	0.63	0.64	0.74	0.72
Min NDVI	0.61	0.61	0.62	0.66	0.77	0.74
Min S2WI	0.63	0.63	0.62	0.59	0.71	0.68

Table 4: Pearson's Correlation Coefficient between BSC and reference reflectance values, for different compositing methods. The BSCs resulted from 1-year long L8 time series (2015). Minimum number of BS instances was set to 2. Fixed threshold values: 0<NDVI< 0.30, 0<NBR2 < 0.1, -1 <BSI <1, -0.8<S2WI<0, maximum 30% cloud cover.

Next the use of dynamic (Dy) thresholding to differentiate BS while employing 1-year or 6-year long L8 time series is evaluated. In Table 5 comparison of BSC's reflectance with the reference data for BSCs with or without dynamic thresholding with different indices and combinations of them is presented (1-year BSC). The fixed threshold for NDVI is set to 0.30. While no dynamic thresholding (fixed thresholding applied only) yielded good results, the application of it (fixed thresholding and then dynamic thresholding applied) with either index or combination of indices did not improve the correlation with the reference data and significantly reduced the coverage. That is due to the minimum number of BS instances constraint applied after the dynamic thresholding. It is worth noting that the RMSE is lower for the BSCs with DyBSI (fixed thresholding and then dynamic thresholding with BSI applied) and higher for the BSCs with DyS2WI, compared to the fixed thresholding BSC. Upon visual investigation, we observed that high BSI values generally correspond to pixels with higher reflectance values (brighter), while low S2WI values correspond to pixels with lower reflectance values (darker) in our study area.

Similarly, in Table 6 comparison of BSC's reflectance with the reference data for BSCs with or without dynamic thresholding with different indices and combinations of them is presented (6-year BSC). The fixed threshold for NDVI is set to 0.30. When dynamic thresholding is applied for each of the three indices alone (i.e. DyBSI, DyNBR2, DyS2WI) the coverage of the BSC is moderately reduced but in some cases the correlation and RMSE are improved. DyBSI yielded better correlation with the reference data on the NIR and SWIR part of the spectrum and overall lower RMSE. With the exception of a lower correlation in the visible-near-infrared (VNIR) part of the spectrum, DyNBR2 achieved results that were generally comparable to those of the fixed thresholding. DyS2WI achieved higher correlation than the fixed thresholding method for most of the bands but RMSE values are generally higher.

Using dynamic thresholding on two or more indices simultaneously significantly reduced the coverage of the BSC without improving correlation or RMSE. Especially the combination of DyBSI and DyS2WI, yielded the lowest correlation and has the lowest coverage. These two indices highlight the pixels with highest and lowest reflectance values respectively, so their combination resulted in the elimination of many pixels.

Most of the experiments achieved ubRMSE around 0.03 for the RGB bands and 0.05 for the infrared bands, indicating the residual effect of crop residue and soil moisture.

	Metrics	Blue	Green	Red	NIR	SWIR1	SWIR2	Support
NDVI+NBR2+BSI (No Dynamic Thresholding)	r^2	0.71	0.72	0.71	0.73	0.82	0.79	80
	RMSE	0.05	0.07	0.09	0.10	0.16	0.18	
	ubRMSE	0.02	0.03	0.04	0.05	0.05	0.05	
NDVI+NBR2+BSI + Dy(BSI)	r^2	0.74	0.73	0.67	0.73	0.82	0.78	56
	RMSE	0.04	0.05	0.07	0.07	0.13	0.15	
	ubRMSE	0.02	0.03	0.04	0.04	0.05	0.05	
NDVI+NBR2+BSI + Dy(NBR2)	r^2	0.67	0.66	0.60	0.63	0.74	0.72	56
	RMSE	0.05	0.07	0.09	0.11	0.16	0.18	
	ubRMSE	0.02	0.03	0.04	0.05	0.06	0.05	
NDVI+NBR2+BSI + Dy(S2WI)	r^2	0.68	0.68	0.63	0.64	0.78	0.75	56
	RMSE	0.06	0.08	0.10	0.12	0.18	0.19	
	ubRMSE	0.02	0.03	0.03	0.05	0.05	0.05	
NDVI+NBR2+BSI + Dy(BSI+S2WI)	r^2	0.85	0.82	0.72	0.72	0.84	0.79	9
	RMSE	0.05	0.07	0.09	0.10	0.14	0.16	
	ubRMSE	0.01	0.02	0.03	0.04	0.04	0.04	
NDVI+NBR2+BSI + Dy(NBR2+BSI)	r^2	0.74	0.74	0.68	0.67	0.79	0.74	28
	RMSE	0.04	0.05	0.07	0.08	0.12	0.14	
	ubRMSE	0.02	0.03	0.04	0.05	0.05	0.05	
NDVI+NBR2+BSI + Dy(NBR2+S2WI)	r^2	0.72	0.71	0.66	0.68	0.81	0.78	30
	RMSE	0.06	0.08	0.11	0.13	0.19	0.20	
	ubRMSE	0.02	0.03	0.04	0.05	0.05	0.05	

Table 5: Pearson's Correlation Coefficient, RMSE and ubRMSE between BSC and reference reflectance values, for dynamic thresholding with different indices. The BSCs resulted from 1-year long L8 time series (2015). Minimum number of BS instances was set to 2. Fixed threshold values: 0<NDVI< 0.30, 0<NBR2 < 0.1, -1 <BSI <1, maximum 30% cloud cover.

	Metrics	Blue	Green	Red	NIR	SWIR1	SWIR2	Support
NDVI+NBR2+BSI (No Dynamic Thresholding)	r^2	0.75	0.76	0.74	0.76	0.82	0.80	122
	RMSE	0.06	0.07	0.10	0.10	0.16	0.18	
	ubRMSE	0.02	0.03	0.03	0.04	0.05	0.04	
NDVI+NBR2+BSI + Dy(BSI)	r^2	0.73	0.74	0.73	0.78	0.85	0.81	111
	RMSE	0.05	0.06	0.07	0.07	0.12	0.14	
	ubRMSE	0.02	0.03	0.04	0.04	0.05	0.05	
NDVI+NBR2+BSI + Dy(NBR2)	r^2	0.71	0.71	0.71	0.73	0.82	0.78	111
	RMSE	0.06	0.07	0.09	0.10	0.16	0.17	
	ubRMSE	0.02	0.03	0.04	0.05	0.05	0.05	
NDVI+NBR2+BSI + Dy(S2WI)	r^2	0.75	0.78	0.78	0.76	0.83	0.79	111
	RMSE	0.06	0.08	0.11	0.12	0.18	0.19	
	ubRMSE	0.02	0.03	0.03	0.04	0.05	0.04	
NDVI+NBR2+BSI + Dy(BSI+S2WI)	r^2	0.62	0.62	0.61	0.63	0.77	0.75	58
	RMSE	0.05	0.06	0.08	0.09	0.13	0.15	
	ubRMSE	0.02	0.03	0.03	0.05	0.05	0.05	
NDVI+NBR2+BSI + Dy(NBR2+BSI)	r^2	0.68	0.69	0.69	0.76	0.83	0.78	83
	RMSE	0.04	0.05	0.07	0.07	0.12	0.14	
	ubRMSE	0.02	0.03	0.04	0.04	0.05	0.05	
NDVI+NBR2+BSI + Dy(NBR2+S2WI)	r^2	0.73	0.73	0.71	0.69	0.81	0.79	84
	RMSE	0.06	0.08	0.11	0.12	0.18	0.19	
	ubRMSE	0.02	0.03	0.03	0.04	0.05	0.05	

Table 6: Pearson's Correlation Coefficient, RMSE and ubRMSE between BSC and reference reflectance values, for dynamic thresholding with different indices. The BSCs resulted from 6-year long L8 time series (2015-2020). Minimum number of BS instances was set to 2. Fixed threshold values: 0<NDVI< 0.30, 0<NBR2 < 0.1, -1 <BSI <1, maximum 30% cloud cover.

In Table 7 metrics for the 6-year BSCs with fixed threshold for NDVI set to 0.25 are presented. In this case the relative performance differences between the composites derived with fixed thresholding versus with dynamic thresholding is comparable to those observed with more lenient NDVI threshold (Table 6) but overall, the results are slightly lower.

Comparing the results for the BSC with no dynamic thresholding and stricter NDVI threshold (0.25) to the BSCs with dynamic thresholding and more lenient NDVI threshold (0.30) , it is worth noting that the coverage is similar in both cases (114 and 111 support) but metrics values are improved in the latter case (lenient NDVI threshold, dynamic thresholding), especially in the NIR and SWIR part of the spectrum.

	Metrics	Blue	Green	Red	NIR	SWIR1	SWIR2	Support
NDVI+NBR2+BSI (No Dynamic Thresholding)	r^2	**0.75**	**0.74**	**0.73**	**0.76**	**0.82**	**0.79**	114
	RMSE	**0.06**	**0.07**	**0.10**	**0.11**	**0.16**	**0.18**	
	ubRMSE	0.02	0.03	0.03	0.04	0.05	0.05	
NDVI+NBR2+BSI + Dy(BSI)	r^2	0.71	0.72	0.71	0.77	0.84	0.80	101
	RMSE	0.05	0.06	0.07	0.08	0.12	0.14	
	ubRMSE	0.02	0.03	0.04	0.04	0.05	0.05	
NDVI+NBR2+BSI + Dy(NBR2)	r^2	0.68	0.67	0.67	0.70	0.81	0.77	101
	RMSE	0.05	0.07	0.09	0.10	0.15	0.17	
	ubRMSE	0.02	0.03	0.04	0.05	0.05	0.05	
NDVI+NBR2+BSI + Dy(S2WI)	r^2	0.73	0.76	0.76	0.75	0.82	0.79	101
	RMSE	0.06	0.08	0.11	0.12	0.18	0.19	
	ubRMSE	0.02	0.03	0.03	0.04	0.05	0.04	
NDVI+NBR2+BSI + Dy(BSI+S2WI)	r^2	0.62	0.60	0.58	0.61	0.75	0.72	55
	RMSE	0.05	0.06	0.08	0.09	0.13	0.15	
	ubRMSE	0.02	0.03	0.04	0.05	0.05	0.05	
NDVI+NBR2+BSI + Dy(NBR2+BSI)	r^2	0.68	0.69	0.70	0.74	0.82	0.76	75
	RMSE	0.04	0.05	0.07	0.07	0.12	0.14	
	ubRMSE	0.02	0.03	0.04	0.04	0.05	0.05	
NDVI+NBR2+BSI + Dy(NBR2+S2WI)	r^2	0.70	0.68	0.66	0.65	0.78	0.77	76
	RMSE	0.06	0.08	0.11	0.12	0.18	0.19	
	ubRMSE	0.02	0.03	0.03	0.05	0.05	0.05	

Table 7: Pearson's Correlation Coefficient, RMSE and ubRMSE between BSC and reference reflectance values, for dynamic thresholding with different indices. The BSCs resulted from 6-year long L8 time series (2015-2020). Minimum number of BS instances was set to 2. Fixed threshold values: 0<NDVI< 0.25, 0<NBR2 < 0.1, -1 <BSI <1, maximum 30% cloud cover.

3.2 Soil OC prediction

The resulting BSCs from the 6-year long L8 time series, with fixed thresholding values: 0<NDVI< 0.30, 0<NBR2 < 0.1, -1 <BSI <1, maximum 30% cloud cover, minimum number of BS instances set to 2, and LUCAS 2015 database were selected to create regression models for soil OC prediction, in order to assess how the various indices, via dynamic thresholding, influenced the quality of the BSC. In Table 8 R^2 and RMSE for LR, KR, RF and SVR regression models with the BSCs are presented. A large variability in the results is observed.

Regression Algorithm	LR		KR		RF		SVR		Support
Metrics	R^2	RMSE	R^2	RMSE	R^2	RMSE	R^2	RMSE	
NDVI+NBR2+BSI (No Dynamic Thresholding)	0.01	10.55	-0.27	11.94	-0.77	14.13	-0.09	11.09	122
NDVI+NBR2+BSI + Dy(BSI)	**0.07**	**10.38**	**0.69**	**6.01**	**0.65**	**6.34**	**0.45**	**7.96**	111
NDVI+NBR2+BSI + Dy(NBR2)	-0.08	11.20	**0.73**	**5.56**	**0.17**	**9.81**	**0.55**	**7.23**	111
NDVI+NBR2+BSI + Dy(S2WI)	-0.20	11.79	**0.29**	**9.07**	-0.80	14.43	**0.33**	**8.78**	111
NDVI+NBR2+BSI + Dy(BSI+S2WI)	-0.53	17.07	-0.10	14.48	0.02	13.70	0.03	13.57	58
NDVI+NBR2+BSI + Dy(NBR2+BSI)	0.39	9.37	**0.81**	**5.23**	0.08	11.51	**0.25**	**10.37**	83
NDVI+NBR2+BSI + Dy(NBR2+S2WI)	-5.48	9.68	-7.33	10.98	-3.50	8.06	-19.22	17.10	84

Table 8: Validation results of the soil OC prediction models. The statistics used: R^2 = coefficient of determination; RMSE = root mean square error. LR: Linear Regression, KR: Kernel Ridge Regressor, RF: Random Forest Regressor, SVR: Support Vectors Regressor.

Models based on the BSCs created with DyBSI and DyNBR2 yielded significantly better results compared to the model based on the BSC with fixed thresholding. BSC with DyBSI yielded substantially higher R^2 and lower RMSE than the BSC with fixed thresholding with all models and was the one that had the most stable performance. BSC with DyNBR2 yielded higher R^2 and lower RMSE than the BSC with fixed thresholding with all models, except LR. However, the results were dependent on the regressor used (i.e. R^2 0.73 with the KR regressor but 0.17 with the RF). BSC with DyS2WI yielded moderate R^2 and RMSE when KR or SVR were employed but still these results were better than the BSC with fixed thresholding.

The models derived from the dynamic thresholding with combinations of the indices have lower support and thus are not directly comparable. It is noted that the models based on the Dy NBR2+BSI yielded good results with the KR algorithm, but the performance was not good for the rest of the regressors.

Overall, LR models appeared insufficient to capture the complexity of the problem, as evidenced by their comparatively lower performance. KR and SVR yielded the best performances amongst all BSCs.

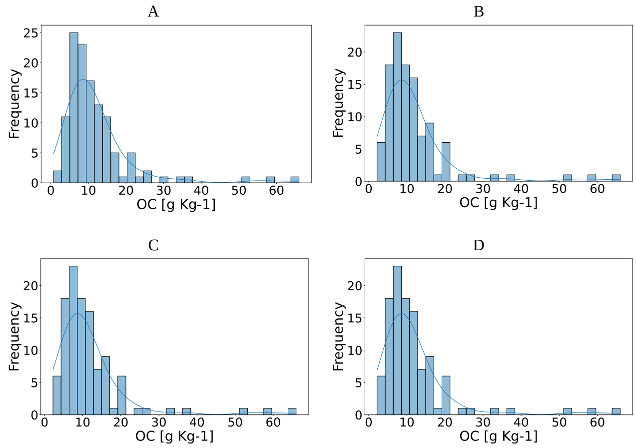

Figure 1: Frequency of Organic Carbon values from the LUCAS 2015 database. The samples that overlay with each BSC. A) NDVI+NBR2+BSI (No Dynamic Thresholding), B) NDVI+NBR2+BSI + Dy(BSI), C) NDVI+NBR2+BSI + Dy(NBR2), D) NDVI+NBR2+BSI + Dy(S2WI).

In Figure 1 the distribution of OC in-situ values of the samples that overlap with each BSC are presented for the experiments with minimally adequate number of samples. The distributions are right skewed with very few samples having OC values greater that 25 g Kg^{-1}. The BSCs created with DyBSI, DyNBR2 or DyS2WI respectively have the same distribution of target values (Figure 1 B, C and D), thus they are directly comparable using R^2 and RMSE. BSC with fixed thresholding includes more samples (122 compared to 111 with the dynamic thresholding) with low values of OC in the in-situ dataset (0-10 g Kg-1).

In Figure 2 the scatterplots of the KR regression experiments with minimally adequate number of samples are presented. All models tend to overestimate low OC values, a pattern that is commonly reported in the literature (Klara Dvorakova P. S., 2020), (Diego Urbina-Salazar, 2023). Notably, the BSC generated with fixed thresholding (Figure 2A) exhibited the most significant overestimation of low OC values among all methods which may indicate insufficient BS masking. While BSC generated with DyBSI (Figure 2B) exhibited the least overestimation of low OC values. Samples with large OC values on the other hand tend to be significantly underestimated for all models, which is also reported by (Tom Broeg, 2024), except when DyBSI or DyNBR2 was used (Figure 2 B and C). Underestimation of larger OC values was observed by (Fabio Castaldi S. C., 2019) when NBR2 threshold value was increased by 0.05 to 0.10. BSCs derived using DyNBR2 or DyBSI facilitated improved performance in this context; however, the limited number of samples with high OC content is constraining.

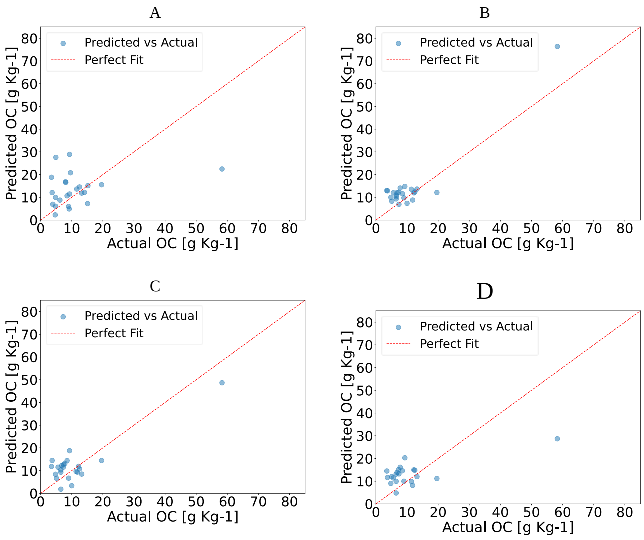

Figure 2: The Kernel Ridge regression scatter plots for each BSC. The samples that overlay with each BSC. A) NDVI+NBR2+BSI (No Dynamic Thresholding), B) NDVI+NBR2+BSI + Dy(BSI), C) NDVI+NBR2+BSI + Dy(NBR2), D) NDVI+NBR2+BSI + Dy(S2WI).

In Figure 3 the Days of Year (DOY) when each thresholding methodology detected BS, for each BSC, is presented. For all methodologies the majority of BS instances is detected in late spring, when fields are prepared for sowing. Fewer BS instances are detected in the summer when most crops are growing, and fields are covered in vegetation. DyBSI (Figure 3 B) detects the least amount of BS instances in autumn, when crops are harvested and a lot of crop residue is present, and in the winter, when soil moisture is high. This may explain the good performance of this methodology regarding correlation with reference data and soil OC prediction models. DyNBR2+BSI methodology (Figure 3 F) also detects very few BS instances in autumn and in winter which may explain the good performance with KR regressor but since the sampling points where few, due to limited coverage, the performance was unstable when considering all regressors. Overall BSCs with prevalent late spring reflectance seems to have the best correlation with LUCAS 2015 database data.

DyNBR2 (Figure 3 C) detects more instances in early spring which may indicate the ability of NBR2 to detect crop residue-free BS pixels but also detects more instances in the winter when soil moisture is prevalent. It also detects very few in the summer which may indicate the ability of the method to also detect green vegetation. Fixed thresholding methodology (Figure 3 A) detects more BS instances in the summer than any other methodology, which indicates that fixed thresholding alone may not be adequate to identify BS pixels with no green vegetation. It also detects a lot of BS pixels in the winter when soil moisture is prevalent. These may explain the low performance of the fixed thresholding BSC in the soil OC prediction models (Table 8). DyS2WI methodology detects the most amount of BS pixels in the winter which may explain the lower performance compared to DyBSI or DyNBR2, since LUCAS 2015 in-situ data represent soil reflectance without disturbing factors such as soil moisture (Gergely Tóth, 2013).

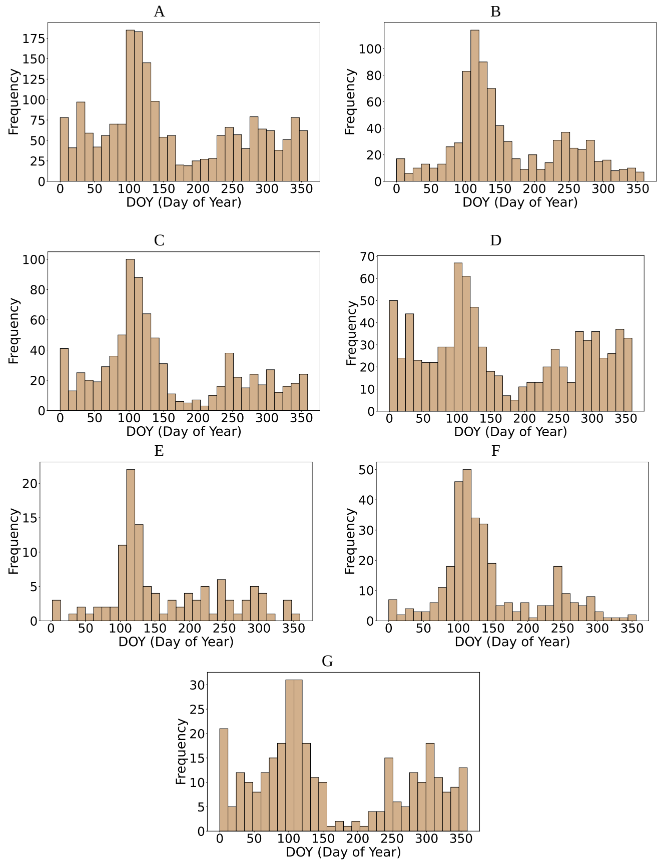

Figure 3: Dates, in DOY form, when BS was detected by every methodology. A) NDVI+NBR2+BSI (No Dynamic Thresholding), B) NDVI+NBR2+BSI + Dy(BSI), C) NDVI+NBR2+BSI + Dy(NBR2), D) NDVI+NBR2+BSI + Dy(S2WI), E) NDVI+NBR2+BSI + Dy(BSI+S2WI), F) NDVI+NBR2+BSI + Dy(NBR2+BSI) and G) NDVI+NBR2+BSI + Dy(NBR2+S2WI).

DyBSI+S2WI (Figure 3 E) detects very few BS pixels in the winter but relatively large amount of BS pixels in the summer. It is possible that it can detect low soil moisture pixels but misses the green vegetation information. In any case the number of samples is too low to accurately explain the performance of this BSC regarding soil OC prediction. DyNBR2+S2WI (Figure 3 G) displays a very similar DOY distribution to DyNBR2 but detects more BS pixels during the winter. It is also the one with the most spread distribution of DOYs in the year.

In Figure 4 the NDVI+NBR2+BSI+DyBSI BSC for the entire country is presented (6-year long L8 time series, with fixed thresholding values: 0<NDVI< 0.30, 0<NBR2 < 0.1, -1<BSI <1, maximum 30% cloud cover, minimum number of BS instances set to 2). All the main agricultural plains of Greece are covered by the BSC and are visible in the top map. Grey denotes areas where no BS was detected, and this is mainly due to forests or built-up areas. It is also noted that areas where mainly olive grove trees or fruit trees are cultivated have very little coverage as expected.

In the bottom part of Figure 4, parts of two large agricultural plains (Thessalian plain and Thessaloniki plain) are presented. The agricultural fields have good coverage while the no data areas are mainly built-up areas, forests and rivers. The resulting

BSC has a uniform appearance and localized colour variations across different areas and regions are visible.

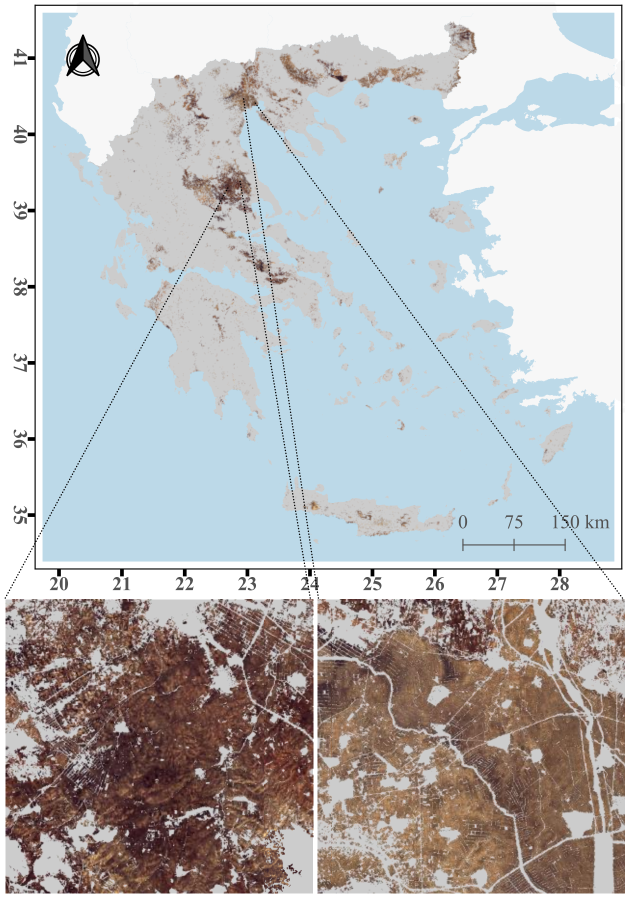

Figure 4: Bare Soil Composite (BSC), natural colour composite (RGB-432), Greece (top), Thessalian agricultural plain (bottom left) and Thessaloniki agricultural plain (bottom right). Grey denotes no data (pixels where no BS was detected).

4. Conclusions

This study highlights that careful selection of the parameters used to create a Bare Soil Composite can significantly improve its quality and performance for accurate soil mapping. We tested the performance of various widely used spectral indices for BS identification and results showed that simultaneous use of indices yielded better results. Setting a minimum number of BS observations had great impact on the quality of the resulting BSC. Dynamic thresholding demonstrated significant potential for accurately identifying bare soil (BS) while maintaining high coverage. The use of different spectral indices in a dynamic thresholding setting, led to the dominance of different seasons in the resulting BSCs, thereby influencing the prevailing reflectance characteristics, which is crucial for effective BS mapping. (Emmanuelle Vaudour C. G., 2019), (Klara Dvorakova U. H., 2021). Dynamic thresholding did not improve the accuracy when 1-year of L8 data was used, possibly due to very low bare soil frequency but proved beneficial when 6 years were used. The best compositing methods in terms of correlation with the reference data, were the mean and median methods. These BSCs had also minimum salt and pepper noise which is a known issue (José Alexandre Melo Demattê, 2018). Maximum cloud cover threshold applied for filtering L8 timeseries did not notably increased the coverage of the BSCs.

Although the number of usable in-situ measurements in the LUCAS 2015 database was low for modelling soil OC over the entire Greece which is characterized by very diverse conditions, a lot of different soil groups, where many different crops are cultivated with different cultivation technics, a preliminary evaluation of the performance of the BSCs for such task was attempted. Aim of this study was to find whether the resulting BSCs can potentially contain valuable information towards OC estimation. Results showed the improvement of the model's performance when dynamic thresholding with certain spectral indices was used and common issues like over/under estimation of OC predicted values were mitigated but further investigation with more exhaustive training dataset is needed in the future.

All in all, this work targeted the accurate bare soil reflectance mapping in Greece at medium spatial resolution by benchmarking the performance of various compositing approaches, while providing a thorough assessment of the contribution of different techniques. We demonstrated that estimating bare soil reflectance from multispectral satellite image time series can be significantly improved through careful selection and optimization of a wide range of parameters. The results offer a strong basis for refining methodologies in bare soil reflectance estimation over large heterogeneous areas and provide insightful information for future monitoring efforts aimed at supporting sustainable soil management and combating soil degradation globally.

Acknowledgements

The authors are supported by the European Research Council (ERC) under the European Union's Horizon 2020 research and innovation program (Grant Agreement No. 101135358).

References

Broeg, T., Don, A., Gocht, A., Scholten, T., Taghizadeh-Mehrjardi, R., Erasmi, S., 2024. Using local ensemble models and Landsat bare soil composites for large-scale soil organic carbon maps in cropland. Geoderma, 444, 116850. https://url.org/10.1016/j.geoderma.2024.116850.

Castaldi, F., 2021. Sentinel-2 and Landsat-8 Multi-Temporal Series to Estimate Topsoil Properties on Croplands. Remote Sensing, 13(17). 10.3390/rs13173345.

Castaldi, F., Chabrillat, S., Don, A., van Wesemael, B., 2019. Soil Organic Carbon Mapping Using LUCAS Topsoil Database and Sentinel-2 Data: An Approach to Reduce Soil Moisture and Crop Residue Effects. Remote Sensing, 11(18). 10.3390/rs11182121.

Castaldi, F., Halil Koparan, M., Wetterlind, J., Žydelis, R., Vinci, I., Özge Savaş, A., Kıvrak, C., Tuncay, T., Volungevičius, J., Obber, S., Ragazzi, F., Malo, D., Vaudour, E., 2023. Assessing the capability of Sentinel-2 time-series to estimate soil organic carbon and clay content at local scale in croplands. ISPRS Journal of Photogrammetry and Remote Sensing, 199, 40-60. https://url.org/10.1016/j.isprsjprs.2023.03.016.

Delaney, B., Tansey, K., Whelan, M., 2025. Satellite Remote Sensing Techniques and Limitations for Identifying Bare Soil. Remote Sensing, 17(4). 10.3390/rs17040630.

Demattê, J. A. M., Fongaro, C. T., Rizzo, R., Safanelli, J. L., 2018. Geospatial Soil Sensing System (GEOS3): A powerful data mining procedure to retrieve soil spectral reflectance from satellite images. Remote Sensing of Environment, 212, 161- 175. https://url.org/10.1016/j.rse.2018.04.047.

Diek, S., Fornallaz, F., Schaepman, M. E., De Jong, R., 2017. Barest Pixel Composite for Agricultural Areas Using Landsat Time Series. Remote Sensing, 9(12). 10.3390/rs9121245. Dvorakova, K., Heiden, U., vanWesemael, B., 2021. Sentinel-2 Exposed Soil Composite for Soil Organic Carbon Prediction. Remote Sensing, 13(9). 10.3390/rs13091791.

Dvorakova, K., Shi, P., Limbourg, Q., van Wesemael, B., 2020. Soil Organic Carbon Mapping from Remote Sensing: The Effect of Crop Residues. Remote Sensing, 12(12). 10.3390/rs12121913.

Gasmi, A., Gomez, C., Lagacherie, P., Zouari, H., Laamrani, A., Chehbouni, A., 2021. Mean spectral reflectance from bare soil pixels along a Landsat-TM time series to increase both the prediction accuracy of soil clay content and mapping coverage. Geoderma, 388, 114864. https://url.org/10.1016/j.geoderma.2020.114864.

Gomez, C., Vaudour, E., Féret, J.-B., de Boissieu, F., Dharumarajan, S., 2022. Topsoil clay content mapping in croplands from Sentinel-2 data: Influence of atmospheric correction methods across a season time series. Geoderma, 423, 115959. https://url.org/10.1016/j.geoderma.2022.115959.

Gorelick, N., Hancher, M., Dixon, M., Ilyushchenko, S., Thau, D., Moore, R., 2017. Google Earth Engine: Planetary-scale geospatial analysis for everyone. Remote Sensing of Environment, 202, 18-27. https://url.org/10.1016/j.rse.2017.06.031. Big Remotely Sensed Data: tools, applications and experiences.

Heiden, U., d'Angelo, P., Schwind, P., Karlshöfer, P., Müller, R., Zepp, S., Wiesmeier, M., Reinartz, P., 2022. Soil Reflectance Composites—Improved Thresholding and Performance Evaluation. Remote Sensing, 14(18). 10.3390/rs14184526.

Karakizi, C., K. Z. V. A. D., Karantzalos, K., 2021. JOINT LAND COVER AND CROP TYPE MAPPING USING MULTI-TEMPORAL SENTINEL-2 DATA FROM VARIOUS ENVIRONMENTAL ZONES IN GREECE. Int. Arch. Photogramm. Remote Sens. Spatial Inf. Sci., XLIII-B3- 2021, 319-326. https://url.org/10.5194/isprs-archives-XLIIIB3- 2021-319-2021, 2021.

KARAKIZI, C., KARANTZALOS, K., KANDYLAKIS, Z., 2024. Exploiting Multitemporal Multispectral High-resolution Satellite Data toward Annual Land Cover and Crop Type Mapping. John Wiley Sons, Ltd, chapter 3, 81–122. https://doi.org/10.1002/9781394306657.ch3

Karakizi, C., Karantzalos, K., Vakalopoulou, M., Antoniou, G., 2018. Detailed Land Cover Mapping from Multitemporal Landsat-8 Data of Different Cloud Cover. Remote Sensing, 10(8). 10.3390/rs10081214.

OPEKEPE, A. U. o. T., 2015. Soil Map of Greece. European Soil Data Centre (ESDAC), Joint Research Centre (JRC). https://esdac.jrc.ec.europa.eu/content/soil-map-greece-0.

Panagos, P., Broothaerts, N., Ballabio, C., Orgiazzi, A., De Rosa, D., Borrelli, P., Liakos, L., Vieira, D., Van Eynde, E., Arias Navarro, C., Breure, T., Fendrich, A., Königer, J., Labouyrie, M., Matthews, F., Muntwyler, A., Jimenez, J. M., Wojda, P., Yunta, F., Marechal, A., Sala, S., Jones, A., 2024. How the EU Soil Observatory is providing solid science for healthy soils. European Journal of Soil Science, 75(3), e13507. https://doi.org/10.1111/ejss.13507.

Safanelli, J. L., Chabrillat, S., Ben-Dor, E., Demattê, J. A. M., 2020. Multispectral Models from Bare Soil Composites for Mapping Topsoil Properties over Europe. Remote Sensing, 12(9). 10.3390/rs12091369.

Hellenic National Meteorological Service, H. N. M., 2025. The climate of Greece. https://emy.gr/the-climate-of-greece.

Silvero, N. E. Q., Demattê, J. A. M., Amorim, M. T. A., dos Santos, N. V., Rizzo, R., Safanelli, J. L., Poppiel, R. R., de Sousa Mendes, W., Bonfatti, B. R., 2021. Soil variability and quantification based on Sentinel-2 and Landsat-8 bare soil images: A comparison. Remote Sensing of Environment, 252, 112117. https://url.org/10.1016/j.rse.2020.112117.

Tóth, G., J. A. M. L., 2013. The LUCAS topsoil database and derived information on the regional variability of cropland topsoil properties in the European Union. Environ Monit Assess, 185(7409–7425). https://doi.org/10.1007/s10661-013-3109-3.

Urbina-Salazar, D., Vaudour, E., Richer-de Forges, A. C., Chen, S., Martelet, G., Baghdadi, N., Arrouays, D., 2023. Sentinel-2 and Sentinel-1 Bare Soil Temporal Mosaics of 6-Year Periods for Soil Organic Carbon Content Mapping in Central France. Remote Sensing, 15(9). 10.3390/rs15092410.

Vaudour, E., Gomez, C., Lagacherie, P., Loiseau, T., Baghdadi, N., Urbina-Salazar, D., Loubet, B., Arrouays, D., 2021. Temporal mosaicking approaches of Sentinel-2 images for extending topsoil organic carbon content mapping in croplands. International Journal of Applied Earth Observation and Geoinformation, 96, 102277. https://url.org/10.1016/j.jag.2020.102277.

Vaudour, E., Gomez, C., Loiseau, T., Baghdadi, N., Loubet, B., Arrouays, D., Ali, L., Lagacherie, P., 2019. The Impact of Acquisition Date on the Prediction Performance of Topsoil Organic Carbon from Sentinel-2 for Croplands. Remote Sensing, 11(18). 10.3390/rs11182143.

Xue, J., Zhang, X., Huang, Y., Chen, S., Dai, L., Chen, X., Yu, Q., Ye, S., Shi, Z., 2024. A two-dimensional bare soil separation framework using multi-temporal Sentinel- 2 images across China. International Journal of Applied Earth Observation and Geoinformation, 134, 104181. https://url.org/10.1016/j.jag.2024.104181.

Zepp, S., Heiden, U., Bachmann, M., Möller, M., Wiesmeier, M., van Wesemael, B., 2023. Optimized bare soil compositing for soil organic carbon prediction of topsoil croplands in Bavaria using Landsat. ISPRS Journal of Photogrammetry and Remote Sensing, 202, 287-302. https://url.org/10.1016/j.isprsjprs.2023.06.003.